Functionalization of 2″-*C*-(Piperazinomethyl)-2′,3′-BcNA (Bicyclic Nucleic Acids) with Pyren-1-ylcarbonyl Units

by **Morten Borre Hansen**[1]), **Nicolai Krog Andersen**[2]), **Michael Raunkjær**[1]), **Per Trolle Jørgensen**, and **Jesper Wengel***

Nucleic Acid Center, Department of Physics, Chemistry and Pharmacy, University of Southern Denmark, Campusvej 55, DK-5230 Odense M (phone: +45-65-502510; e-mail: jwe@sdu.dk)

Herein, we describe the incorporation of 2″-*C*-(piperazinomethyl)-2′,3′-BcNA (Bicyclic Nucleic Acids) into oligonucleotides *via* phosphoramidite chemistry and their subsequent solid-phase functionalization with pyren-1-ylcarbonyl units after oligonucleotide synthesis. Thermal denaturation measurements showed that one modification led to increased thermal stability of the resulting duplex, and that two modifications could be incorporated in close proximity without decreasing the duplex stability (compared to the duplex stability of unmodified RNA). Fluorescence studies of the modified duplexes revealed that the structure and intensity of the fluorescence spectra were largely sequence-dependent. Furthermore, molecular-modeling studies showed that the pyrene moieties are placed in the major groove, and that the configuration at C(2″) is important for the thermal stability of the duplex.

Introduction. – Modification of nucleotides has received significant interest within a multitude of research areas, such as gene silencing, molecular diagnostics, molecular electronics, and nanotechnology [1–7]. This has led to the development of a plethora of modified oligonucleotides (ONs) and ON conjugates [8][9] of which the latter have involved several different functionalities, *e.g.*, metal complexes [10–20], lipids [21–23], peptides and proteins [24–30], aromatic groups [31–37], fullerene [38], and bioorganic acids involved in cellular processes [39–41].

The position most frequently used for conjugation of functionalities to ONs is C(5) of the pyrimidine nucleobases, as the chemistry for functionalization of C(5) is very well developed [32][42–47], and as functionalities at C(5) face the major groove where larger functionalities are better accommodated compared to the minor groove. Nevertheless, thermal destabilization of ON duplexes containing functionalities at C(5) is often observed [14][20][21][30][32][40].

Research in our group on bicyclic nucleic acids (BcNAs) and nucleosides has included studies on two diastereoisomeric 4-(pyren-1-ylbutanoyl)piperazin-1-yl-derivatized nucleotide monomers which led to increased binding affinity against complementary DNA and RNA when compared to the corresponding underivatized monomer **Z** (*cf. Scheme*) or the all-DNA reference ON [48]. These derivatives were prepared by incorporation of fully-derivatized phosphoramidite monomers, *i.e.*, monomers already

[1]) Present address: Novo Nordisk, Novo Nordisk Park, DK-2760 Måløv.
[2]) Present address: Novo Nordisk, Niels Steensens vej 1, DK-2820, Gentofte.

containing the pyren-1-ylbutanoyl units attached to the piperazino group before automated ON synthesis.

NMR Studies have indicated that these piperazino functionalities are directed into the major groove of a DNA duplex [49][50]. Based on these observations, we have extended our study in two directions, namely by developing an on-column post-oligomerization conjugation approach, and by incorporating pyren-1-ylcarbonyl instead of pyren-1-ylbutanoyl units into the ONs. Accordingly, we herein describe the incorporation of phosphoramidites **3** and **4** (*cf. Fig. 1*) into ONs and the subsequent functionalization – so-called post-synthetic functionalization [51] – with pyren-1-ylcarboxylic acid. The influence of this functionality on the stability of ON duplexes was investigated by thermal melting studies. Further, we report fluorescent properties of the functionalized ONs and results of molecular-modelling studies.

Results and Discussion. – *Synthesis of ONs.* The required phosphoramidite derivatives **3** and **4** (*cf. Fig. 1*) were prepared as reported in [48] and subsequently incorporated into ten different ONs **ONS1** – **ONS10** (Table S1, *Supporting Information*[3])). The synthesis was carried out with an automated solid-phase DNA-synthesizer according to a standard protocol [52] except that an extended coupling time (15 min) was applied for phosphoramidites **3** and **4**. To verify the sequence of the ONs, a small sample of each of the solid support bound ONs was first treated with aqueous NH_3 to cleave the ONs from their solid. After purification by reversed-phase HPLC, the molecular weights obtained by MALDI-MS were in accordance with those of the desired ONs, and ion-exchange HPLC showed that the ONs had a purity of $>95\%$ (Table S1 and Fig. S21 – S30; *Supporting Information*).

Solid-Phase Functionalization. **ON1** was used in preliminary studies to establish the most favorable conditions for on-column functionalization by reaction with pyren-1-ylcarboxylic acid after completion of the ON sequence. First, Fmoc was removed by treatment with 20% piperidine in DMF yielding **ON11** with a free amine function at the piperazino group which subsequently was converted into the amide by reaction with pyren-1-ylcarboxylic acid to give **ON21** (*Scheme*). To optimize the reaction conditions, we chose three common coupling reagents used in peptide chemistry and performed the reactions in two different solvents. Thus, six different conditions were set up in total (*Table 1*).

After functionalization with a pyren-1-ylcarbonyl group, the ONs were cleaved from the solid support and purified by ion-exchange HPLC. The coupling efficiencies were evaluated by HPLC as follows: the desired product, **ON31** was identified by UV absorption (pyrene absorption at 342 nm) and MALDI-MS analysis, while unreacted oligonucleotide **ONS1** was identified *via* the retention times found earlier (see above). The integrals of the peaks were normalized by means of the extinction coefficients of non-functionalized and functionalized ONs [53][54], and the efficiency of the coupling conditions was determined as the relative amount of **ON31** to the combined amount of **ON31** *and* unreacted **ONS1** (Table S5 and Fig. S9; *Supporting Information*). From *Table 1*, it is clear that HATU (*O*-[7-azabenzotriazol-1-yl]-*N*,*N*,*N*′,*N*′-tetramethyluronium hexafluorophosphate) in DMF was superior to the other coupling conditions. This

[3]) Available upon request from the authors.

Scheme. *ON Synthesis and Functionalization Exemplified by the Synthesis of* **ON31**

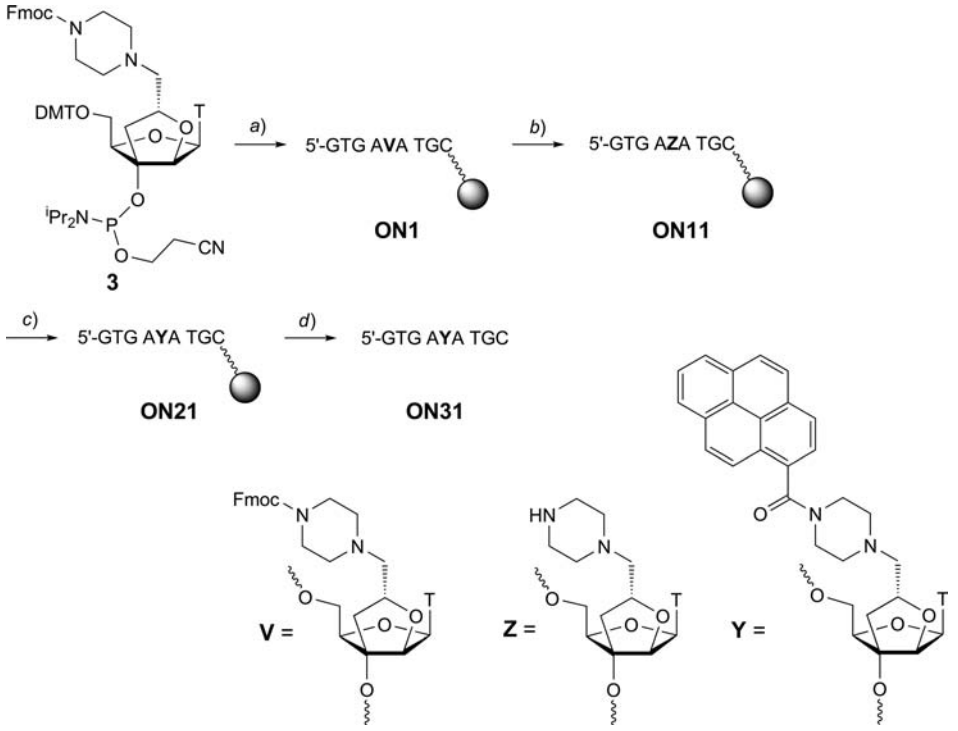

a) DNA Synthesizer. *b*) Piperidine in DMF (20% (*v*/*v*)). *c*) 24 Equiv. of pyren-1-ylcarboxylic acid, 24 equiv. of HATU (= 1-[bis(dimethylamino)methylidene]-1*H*-1,2,3-triazolo[4,5-*b*]pyridinium 3-oxide hexafluorophosphate), HBTU (= *N*,*N*,*N*′,*N*′-tetramethyl-*O*-(1*H*-benzotriazol-1-yl)uronium hexafluorophosphate), or EDC (= 1-ethyl-3-[3-(dimethylamino)propyl]carbodiimide) · HCl, 61 equiv. of $EtN^{i}Pr_2$, CH_2Cl_2 or DMF. *d*) Aq. NH_3 (28–30%, *v*/*v*).

Table 1. *Coupling Efficiencies of the Amide Synthesis Evaluated by HPLC*[a])

Coupling reagent	DMF	CH_2Cl_2
HATU	86%	56%
HBTU	75%	0%
EDC · HCl	0%	0%

[a]) Extinction coefficients ($mol^{-1}\,l\,cm^{-1}$) used: $9.87 \cdot 10^4$ and $1.21 \cdot 10^5$ for unreacted **ONS1** and **ON31**, respectively. All samples were > 95% pure (ion-exhange HPLC).

result is in accordance with experiences from peptide chemistry, in which HATU is recognized as an efficient coupling reagent compared to EDC · HCl and HBTU [55]. Thus, by employing this efficient HATU/DMF system, oligonucleotides **ON32** – **ON40** were prepared by functionalization of **ON12** – **ON20** with pyren-1-ylcarbonyl. These functionalized ONs were cleaved from their solid supports and purified as described above.

Thermal Stability and Molecular Modeling of Modified Duplexes. The oligonucleotides **ON31**–**ON40** were annealed to complementary DNA or RNA strands, and the thermal stabilities (T_m values) of the resulting duplexes were determined (*Table 2*). Further, oligonucleotides **ON31**, **ON32**, **ON37**, and **ON38**, were subjected to a 10-ns SD (stochastic dynamics) simulation. Matching each ON against DNA and RNA complements was studied to rationalize the observed trends in thermal stability effects. In all cases except one, ONs containing a monomer **X** or **Y** (*Fig. 1*) exhibited increased thermal affinities towards complementary DNA. In addition, duplexes containing monomer **X** were thermally more stable than the corresponding duplexes containing monomer **Y** (ΔT_m +1.0 to +7.5° and ΔT_m −1.0 to +5.0° relative to unmodified reference strands Ref. A or Ref. B, resp.). Thermal affinities towards complementary DNA decreased for all ONs containing monomer **Y** (ΔT_m −4.5 to −1.5°). However, ONs modified with monomer **X** showed either decreased (*Entry 4*; *Table 2*) or increased (*Entries 2* and *6*; *Table 2*) thermal affinities towards complementary DNA, but always higher affinities than those observed for the corresponding ONs containing monomer **Y**. Interestingly, **ON36** provides an exception to the general trend that ONs modified with a single monomer **X** or **Y** exhibit selectivity towards DNA (*Entry 6*; *Table 2*).

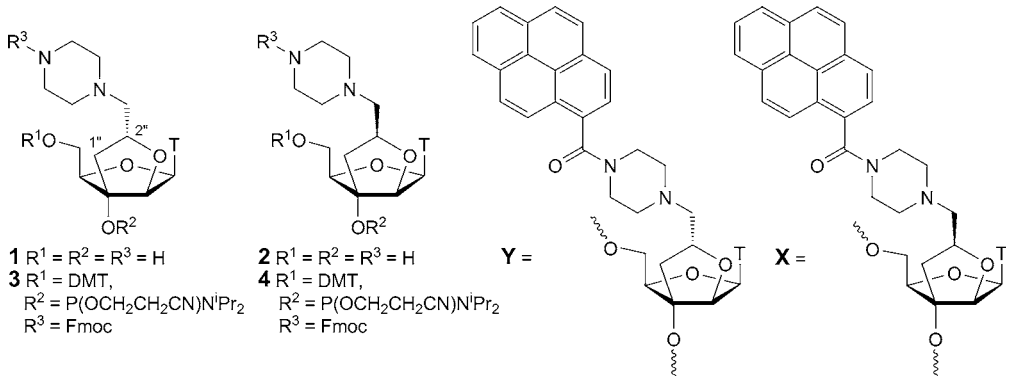

Fig. 1. *Structures of (2″*R*)-2″-*C*-(piperazino)methyl-2′,3′-BcNA*, **1**, *and (2″*S*)-2″-*C*-(piperazino)methyl-2′,3′-BcNA*, **2**, *and their corresponding phosphoramidites* **3** *and* **4**, *which were used to incorporate post-synthetically the modifications* **X** *and* **Y**, *respectively, into ONs.* Fmoc = [(9*H*-fluoren-9-yl)methoxy]carbonyl; DMT = 4,4′-dimethoxytrityl (= bis(4-dimethoxyphenyl)(phenyl)methyl) and T = thymin-1-yl.

These results clearly show that the local geometry of the modification has a large influence on the thermal stability of the modified duplexes. These findings are supported by molecular-modeling simulations, in which both monomers **X** and **Y** were found to perturb the helical structure extensively (Table S6–S9, *Supporting Information*). Apparently, duplexes containing monomer **Y** cannot accommodate the pyrene moiety as well in the major groove as can the corresponding duplexes containing monomer **X**. From molecular-modeling studies of **ON38** (*Fig. 2*) and **ON37** (*Fig. 3*), it can be rationalized that the configuration at C(2″) plays a determining role in the placement of the piperazino ring, which, in the case of monomer **Y**, is placed very close

Table 2. *ONs Synthesized and Thermal Denaturation Studies*[a])

Entry		Sequence	RNA Target		DNA Target	
			T_m [°]	ΔT_m/mod. [°]	T_m [°]	ΔT_m/mod. [°]
	Ref. A	5′-GTG ATA TGC	28.0[b])	–	26.5	–
1	**ON31**	5′-GTG A**Y**A TGC	33.0	+5.0	24.5	−1.5
2	**ON32**	5′-GTG A**X**A TGC	35.5	+7.5	29.0	+2.5
	Ref. B	5′-GCA TAT CAC	28.0[b])	–	27.0	–
3	**ON33**	5′-GCA **Y**AT CAC	31.5	+3.5	22.5	−4.5
4	**ON34**	5′-GCA **X**AT CAC	32.0	+4.0	25.5	−1.5
5	**ON35**	5′-GCA TA**Y** CAC	27.0	−1.0	23.5	−3.5
6	**ON36**	5′-GCA TA**X** CAC	29.0	+1.0	30.0	+3.0
7	**ON37**	5′-GCA **Y**A**Y** CAC	29.0	+0.5	20.5	−3.3
8	**ON38**	5′-GCA **X**A**X** CAC	30.5	+1.3	33.5	+3.3
	Ref. C	5′-GCA ATT CAC	30.5	–	–	–
9	**ON39**	5′-GCA A**YY** CAC	27.0	−3.5	–	–
10	**ON40**	5′-GCA A**XX** CAC	31.0	+0.5	–	–

[a]) Melting temperature T_m (T_m values in [°] (ΔT_m, change in T_m calculated relative to Ref. A, Ref. B, and Ref. C reference duplexes)) measured as the maximum of the first derivative of the melting curve (A_{260} *vs.* temperature) recorded in medium salt buffer ([Na^+] = 110 mM), [Cl^-] = 100 mM, [EDTA] = 0.1 mM, pH 7.0 (NaH_2PO_4/Na_2HPO_4) using 1.0 μM concentrations of each complementary strand. T_m Values are averages of at least two measurements. [b]) Ref. A, 5′-GTG ATA TGC, and Ref. B, 5′-GCA TAT CAC, are complementary.

to the phosphordiester backbone. As a result, duplexes containing monomer **Y** become distorted, which is also reflected in the observed χ and phase angles (Table S6–S9, *Supporting Information*), with the latter deviating from the native S-type for DNA ($0° \pm 36$) and N-type for RNA ($180° \pm 36$) into a more E-type conformation with a phase angle around 150°. A similar trend was observed for the duplexes containing monomer **X**, but to a lesser extent. The data obtained for the glycosidic torsion angle (χ) reflect the overall helical changes in the formed duplexes, and that the base pairing between the adjacent nucleobases becomes less favorable upon incorporating monomer **Y**.

Interestingly, increasing the number of modifications from one to two – either as neighbors (*Entries 9* and *10*; *Table 2*) or next-neighbors (*Entries 7* and *8*; *Table 2*) – revealed that the effects of the modifications on duplex thermal stability are not additive (compare *Entries 4* and *6* with *8*, as well as *3* and *5* with *7*; *Table 2*).

Interestingly, the thermally least stable RNA duplex contains two monomers **Y** as neighbors (*Entry 9*; *Table 2*). The corresponding duplex modified with monomer **X** shows virtually unchanged thermal stability relative to the reference duplex, supporting the assumption that geometrical constraints are responsible for decreased thermal stabilities of duplexes containing **Y** monomers. Similarly, unfavorable steric factors may be responsible for the generally lower thermal denaturation temperatures obtained when compared with those previously reported for the corresponding pyren-1-ylbutanoyl derivatives [48].

Mismatch Discrimination Study. The ability of monomers **X** and **Y** to discriminate between matched and mismatched bases was studied by introducing non-complemen-

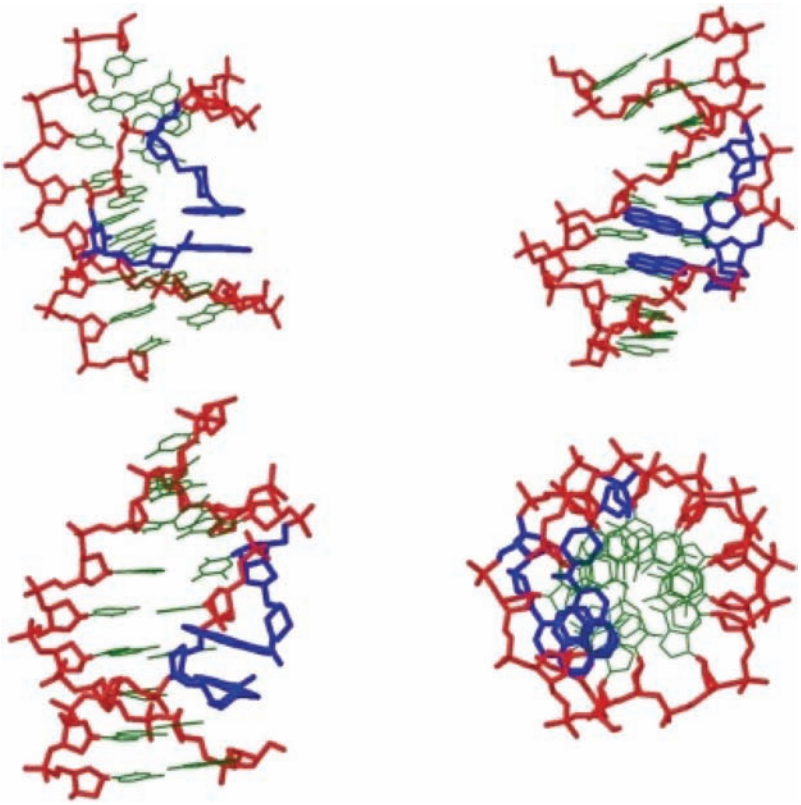

Fig. 2. *Modeling of* **ON38** vs. *DNA* showing representative snapshots of side and top views of the duplex. Color scheme: red, phosphodiester backbone, green, nucleobases, and blue, modification **X**.

tary bases (mismatches) directly opposite to the monomers (*Entries 2*, *3*, *8* and *9*; *Table 3*). Both monomers **X** and **Y** exhibited excellent discrimination abilities, as evidenced by the reduced thermal stabilities of mismatched duplexes (*Entries 2* and *3*; *Table 3*). In both cases, mismatch discrimination was improved relative to that of unmodified DNA (*Entry 1*; *Table 3*).

The mismatch-discriminating ability of monomers **X** and **Y** diverged when a mismatched base pair was introduced between a pair of next-neighbor modifications (*Entries 5* and *6*; *Table 3*). In the case of monomer **Y**, mismatch discrimination was comparable, to or slightly improved relative to, unmodified DNA, while monomer **X** exhibited a reduced discrimination. This suggests that incorporation of monomer **X** as a pair of next-neighbors around a mismatched base pair is accompanied by a drastic structural reorganization of this region, thereby counteracting the destabilizing effect of the mismatch, *e.g.*, by intercalating the pyrene moiety into the core of the duplex.

Decreased mismatch discrimination of modified ONs was also observed when mismatches were introduced opposite to two neighboring modifications. In the case of monomer **Y**, virtually no mismatch discrimination was observed (in fact, stabilization was observed for a **Y**:-dC mismatch). A rearrangement similar to the one suggested for

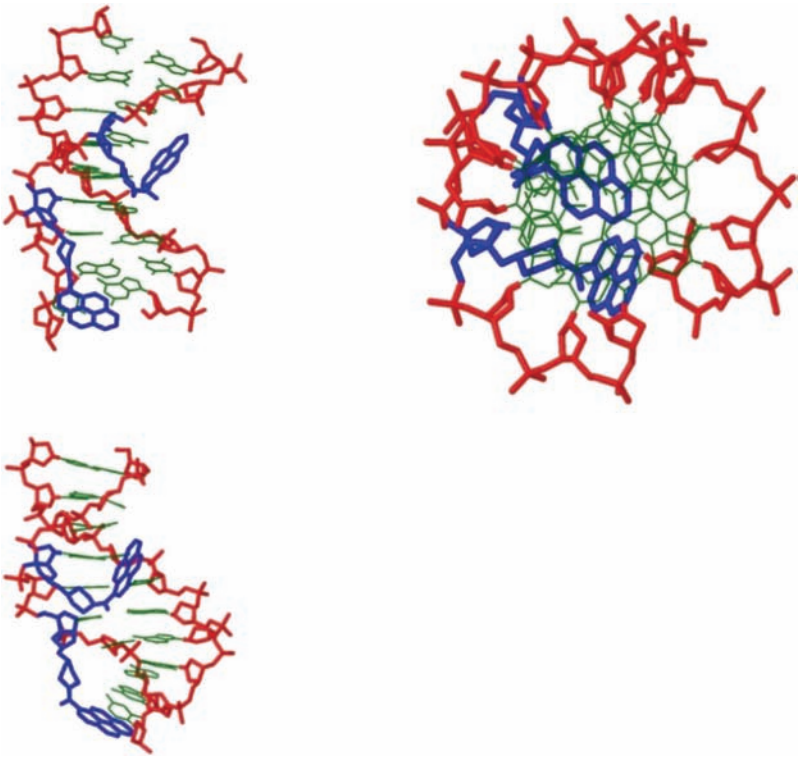

Fig. 3. *Modeling of* **ON37** vs. *DNA* showing representative snapshots of side and top views of the duplex. Color scheme; red, phosphodiester backbone, green, nucleobases, and blue, modification **Y**.

a next-neighboring pair of monomers **X** may apply to two neighboring **Y** monomers. Relief of unfavorable steric interactions may also be a contributing factor, since destabilization relative to unmodified DNA was observed in the corresponding matched duplex.

Fluorescence Spectroscopy of Singly Modified ONs. Fluorescence studies of ONs containing a single monomer **X** or **Y** revealed that the various ONs have very diverse fluorescent properties. First of all, the sequence context seems to be the major determining factor regarding fluorescence, as is evident from the series **ON31**, **ON33**, and **ON35** (*Fig. 2*, *a*–*c*; or **ON32**, **ON34**, and **ON36**; Fig. S2, *Supporting Information*). These ONs displayed rather distinctive fluorescence spectra, notwithstanding that all ONs contain the same modification, **Y** (or **X**) only at different positions in the same nucleotide sequence. For example, duplexes (RNA and DNA) containing **ON31** exhibited unstructured fluorescence spectra, whose intensities were about five times higher than those of single stranded **ON31**. This is supported by the molecular modeling, which shows the singly modified **ON31** and **ON32** targeted against both complementary DNA and RNA to have their modifications (**X** of **Y**) placed in the major groove and thereby in a largely polar environment (Fig. S5–S8, *Supporting Information*). However, even though the modification is placed in the major groove the

Table 3. Thermal Mismatch Discrimination Studies[a])

Entry	Target	Duplex	T_m [°]			
			B = A	B = G	B = T	B = C
1	Ref. A	5′-GTG ATA TGC	**28.0**	20.5	13.5	12.5
		3′-CAC TBT ACG				
		Mismatch discrimination[b])	–	– 7.5	– 14.5	– 15.5
2	**ON31**	5′-GTG A**Y**A TGC	**33.0**	23.5	17.0	12.5
		3′-CAC TBT ACG				
		Mismatch discrimination[b])	–	– 9.5	– 16.0	– 20.5
3	**ON32**	5′-GTG A**X**A TGC	**35.5**	24.0	21.5	14.0
		3′-CAC TBT ACG				
		Mismatch discrimination[b])	–	– 11.5	– 14.0	– 21.5
4	Ref. B	5′-GCA TAT CAC	8.0	17.0	**28.0**	20.0
		3′-CGT ABA GTG				
		Mismatch discrimination[b])	– 20.0	– 11.0	–	– 8.0
5	**ON37**	5′-GCA **Y**A**Y** CAC	12.5	14.5	**30.5**	22.0
		3′-CGT ABA GTG				
		Mismatch discrimination[b])	– 18.0	– 16.5	–	– 8.5
6	**ON38**	5′-GCA **X**A**X** CAC	22.0	24.5	**29.0**	23.0
		3′-CGT ABA GTG				
		Mismatch discrimination[b])	– 7.0	– 5.5	–	– 6.0
7	Ref. C	5′-GCA ATT CAC	**30.5**	17.5	14.0	7.5
		3′-CGT TBA GTG				
		Mismatch discrimination[b])	–	– 13.0	– 16.5	– 23.0
8	**ON39**	5′-GCA A**YY** CAC	**27.0**	24.0	25.5	28.5
		3′-CGT TBA GTG				
		Mismatch discrimination[b])	–	– 3.0	– 1.5	+ 1.5
9	**ON40**	5′-GCA A**XX** CAC	**31.0**	18.5	20.5	22.5
		3′-CGT TBA GTG				
		Mismatch discrimination[b])	–	– 12.5	– 10.5	– 8.5

[a]) For conditions of thermal denaturation experiments, see *Table 2*. T_m Values of fully matched duplexes are indicated in bold. [b]) Mismatch discrimination, change in T_m value relative to the fully matched duplex.

sugar ring has limited flexibility, which as a consequence restricts the overall flexibility of the duplex. For **ON35**, the situation was almost the exact opposite; all the spectra were structured, and the single stranded ON displays the most intense fluorescence. A possible explanation of the difference in fluorescence intensities between **ON31** and **ON35** (or **ON32** and **ON36**) may be differences in guanosine quenching. Since **ON31** has a higher guanine content than **ON35** (3/9 *vs.* 1/9), and since guanine nucleobases are known to efficiently quench pyrene fluorescence [56], a greater degree of quenching in single-stranded **ON31** than in **ON35** may explain the lower fluorescence intensity. Even though neither **ON31** nor **ON35** has a neighboring guanine, the high flexibility of single-stranded ONs may bring the pyrene moiety and a guanine nucleobase into close proximity by folding the single stranded ON which may lead to quenching. Along the same lines, the hybridization-induced fluorescence increase observed for **ON31** may be a consequence of the rigidity of the resulting duplex, which prevents folding and quenching by distal guanine nucleobases, or by any other proximal

nucleobase as well. Conversely, hybridization of **ON35** with a complementary ON leads to introduction of a guanine nucleobase next to the pyrene moiety *via* a G · C base pair, which may explain the high degree of quenching of pyrene fluorescence observed in this case.

Interestingly, relative to the corresponding single stranded ONs, all duplexes displayed a marked bathochromic shift in UV spectra of the pyrene absorption maximum (Table S3, *Supporting Information*). This observation indicaties a strong electronic interaction between pyrene and the nucleobases [57], which, in the case of duplexes containing **ON31** – **ON34**, however, did not lead to quenching of the pyrene fluorescence. This interaction, together with the known configuration of the 2″-*C*-(piperazinomethyl)-2′,3′-BcNA skeleton [50], may suggest that pyrene is located in the major groove in close proximity to the nucleobases.

With regard to the configuration of the modification (**X** or **Y**), only the **ON35**/**ON36** pair showed significant differences in their fluorescent properties as a result of the configuration. In this respect, **ON36** was found to be over 2.5 times more fluorescent than single stranded **ON35**. This overall absence of stereochemical influence on fluorescence is in sharp contrast to the thermal denaturation studies, as discussed above, in which clear differences between different stereoisomers were observed. **ON33** and **ON34** fall between the above-mentioned extremes **ON31**/**ON32** and **ON35**/**ON36**, in as much as no significant difference was detacted between single-stranded ONs and duplexes; rather high fluorescence intensity was observed at all times. This coincides with a low guanine content in the single-stranded ONs as well as in the matched duplexes, implying that no significant quenching by guanine or other bases took place.

Mismatch discrimination was also studied using fluorescence (*Fig. 4*, *d*, and Fig. S2, *Supporting Information*). Intense fluorescence was observed for a fully matched duplex, as discussed above (**ON31** and **ON32**; *Entries 2* and *3*; *Table 3*), whereas mismatches led to a drop in fluorescence mirroring the thermal discrimination findings. This mismatch-induced fluorescence decrease may be a result of increased flexibility of the duplex caused by the mismatches, leading to increased quenching by the nucleobases, perhaps by intercalation of the pyrene moiety. The best mismatch discrimination (most pronounced fluorescence decrease) was found for an **X**-C (or **Y**-C) mismatch, and the worst for **X**-T.

Fluorescence Spectroscopy of Doubly Modified ONs. Fluorescence measurements of doubly modified ONs showed a similar or even reduced intensity relative to singly modified ONs (*Fig. 5*, *a* and *b*, and Fig. S3; *Supporting Information*). Besides the normal pyrene emission (bands at 370 – 450 nm), single-stranded ONs and duplexes containing mismatches also showed additional weak, unstructured and broad bands around 450 – 520 nm, presumably caused by pyrene excimers [54]. It is remarkable that the fluorescence intensity did not increase upon doubling the number of pyrene moieties (*i.e.*, **ON7** – **ON10** *vs.* **ON3** – **ON6**). In this respect, **ON10** stands out, since this ON has the lowest overall fluorescence intensity of all ONs in this study, when the total fluorescence of both single-stranded and duplex ONs is considered. Altered local folding motifs leading to increased quenching and excimer fluorescence, which takes place at expense of monomer fluorescence, may be proposed as reasons for the low fluorescence intensities of the doubly modified ONs. Finally, it can be noted that

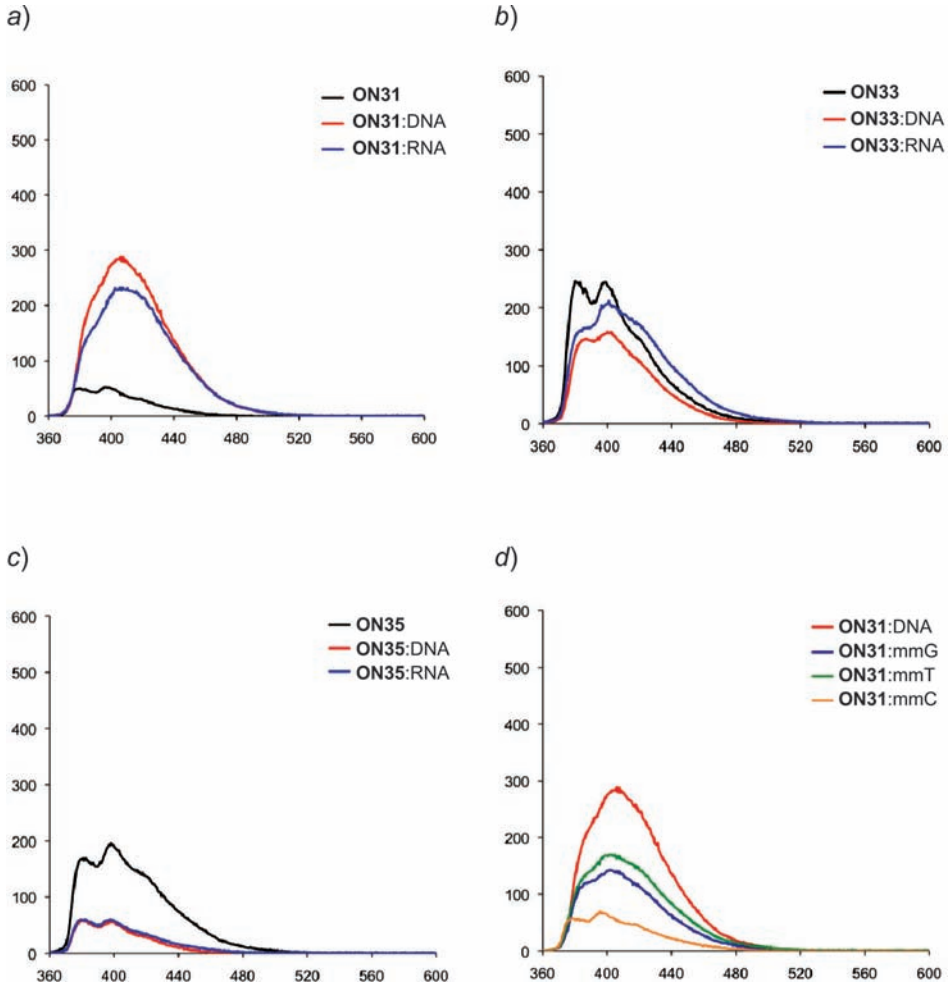

Fig. 4. *Fluorescence spectra of ONs containing a single* **X** *monomer,* **ON31**, **ON33***, and* **ON35** (*a*–*c*), *as well as of* **ON31** *with a matched as well as singly mismatch discrimination of* **ON31** (*d*)

fluorescence-based mismatch discrimination with the doubly modified ONs was rather poor (*Fig. 5*,*c* and *d*, and Fig. S3; *Supporting Information*).

Conclusions. – We have demonstrated that 2″-*C*-(piperazinomethyl)-2′,3′-BcNA incorporated into ONs can be functionalized on-column with a pyren-1-ylcarbonyl group after completion of the ON sequence. This was achieved most efficiently with HATU in DMF, which was one out of six coupling reagent/solvent combinations tested, giving a coupling efficiency of 86%. Thermal denaturation measurements of pyren-1-ylcarbonyl-functionalized 2″-*C*-(piperazinomethyl)-2′,3′-BcNA revealed that the configuration at C(2″) in the BcNA skeleton has a significant influence on the thermal stability of duplexes containing this modification. In this regard, the (*S*)-configured

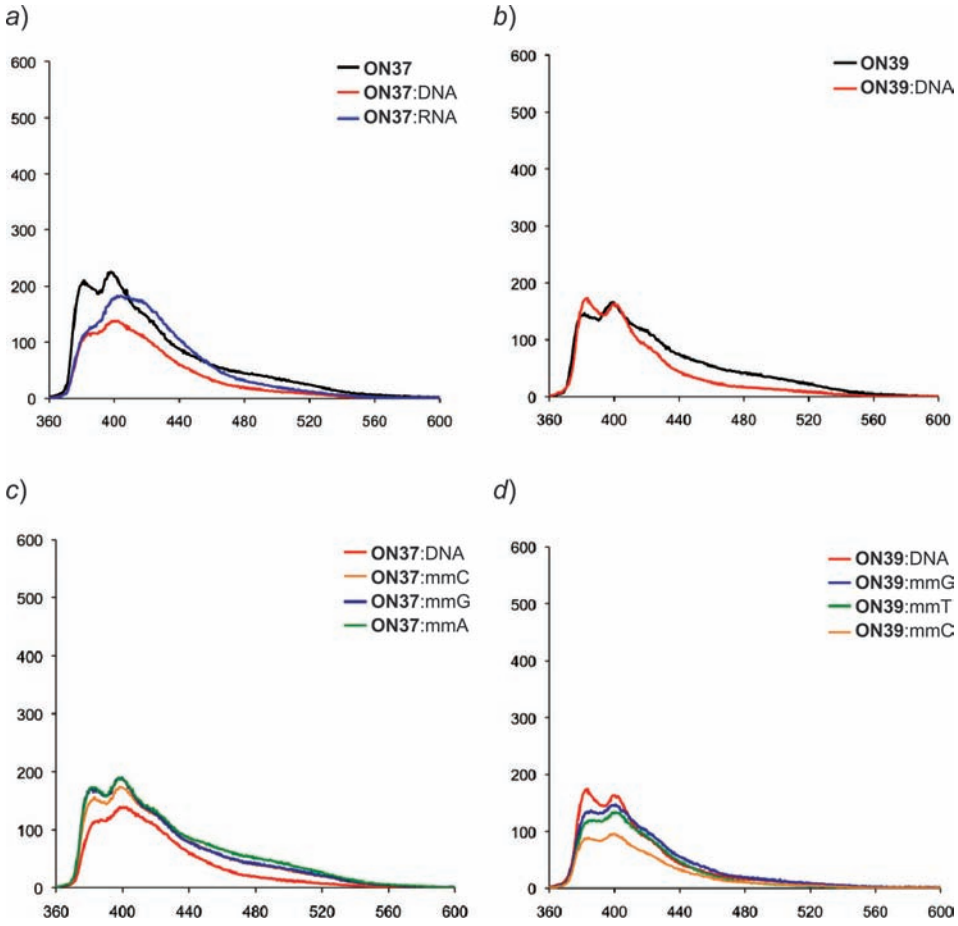

Fig. 5. *Fluorescence spectra of single stranded ONs* **ON37** *and* **ON39** *containing two* **X** *monomers, of their duplexes with DNA and RNA complement* (*a* and *b*)*, and of their duplexes formed with singly mismatched DNA complements* (*c* and *d*)

monomer **X** generally yielded more stable duplexes when compared to the (*R*)-configured monomer **Y**. Moreover, incorporation of two pyrene moieties did not compromise the thermal stability of the resulting duplexes. ONs containing either a single monomer **X** or **Y** showed better thermal discrimination abilities than unmodified ONs. Fluorescence studies of the modified ONs revealed that the structure and intensity of the spectra was dependent on the sequence context in which the pyrene modifications were incorporated, and on the number of modifications. In short, the results obtained confirm the usefulness of 2″-*C*-(piperazinomethyl)-2′,3′-BcNA for positioning larger substituents in the major groove of a DNA double helix.

We thank *Tina Grubbe Hansen* and *Joan Hansen* for performing HPLC analysis and purification of the ONs. The *Danish National Research Foundation* is acknowledged for financial support.

Experimental Part

General. Unmodified oligonucleotides were purchased from *Sigma* in scale of 0.2 μmol, the purity was checked by ion-exchange chromatography and MALDI-TOF mass spectrometry.

Synthesis of ONs **ON1** – **ON10** *and* **ONS1** – **ONS10**. ON Synthesis was carried out on an *Expedite* DNA synthesizer at 1.0-μmol scale using commercial natural DNA phosphoramidites (following a standard protocol) [52] and 2′,3′-BcNA phosphoramidites **3** and **4**. Coupling of the latter was carried out by dissolving the phosphoramidite (22 mg, 20 μmol) in a mixture of anh. MeCN (400 μl) and pyridinium hydrochloride (600 μl, 0.6M), and applying this mixture by passing through the synthesis column during 15 min. After completion of the sequence, final detritylation was omitted. To verify the composition and purity of the ONs, a small fraction of the solid-phase bound ONs (3 mg of the solid phase) was transferred to an *Eppendorf* tube, and the nucleobase protecting groups and solid phase were cleaved off by treatment with aq. NH_3 (1 ml, 28 – 30%) for 16 h at 55°. The remaining solid-phase bound ONs, **ON1** – **ON10**, were saved for subsequent functionalization. The small fractions of **ON1** – **ON10** were filtered and purified by reversed-phase HPLC (gradient shown in Table S10; *Supporting Information*) on a *Waters 600* system equipped with an *Xterra* C_{18} precolumn (10 μm, 7.8 × 10 mm) and an *Xterra* C_{18} column (10 μm, 7.8 × 150 mm). The purified ONs were detritylated by incubation with 80% AcOH for 20 min at r.t. and then precipitated from abs. EtOH at − 18° (14 – 16 h) affording **ONS1** – **ONS10**. The composition of each sample was verified by MALDI-MS analysis (Table S1; *Supporting Information*) and the purity (> 95%) was assessed by anal. ion-exchange HPLC (Fig. S21 – S30; *Supporting Information*) using a *LaChrom* system equipped with a *Dionex* column (4 × 250 mm) (gradient shown in Table S11; *Supporting Information*).

Optimization of ON Functionalization. Solid-phase-bound **ON1** (33 mg of the solid phase) was suspended in 20% piperidine in DMF (1 ml, 20%) in an *Eppendorf* tube and vortexed for 30 min to remove the Fmoc protecting group. Subsequently, the tube was spun at 12,000 rpm for 2 min, and the supernatant was removed. The precipitated material was washed with DMF (2 × 0.5 ml) and MeOH (2 × 0.5 ml), dried on a *SpeedVac*, and divided into six *Eppendorf* tubes (each 5 mg). To three of the tubes, CH_2Cl_2 (80 μl) was added, and to the remaining three DMF (80 μl). Pyrene-1-carboxylic acid in DMF (209 μl, 17.38 mM), HATU in DMF (209 μl, 17.38 mM), HBTU in DMF (209 μl, 17.38 mM), and EDC · HCl in DMF (209 μl, 17.38 mM) were added to each tube containing DMF. Pyrene-1-carboxylic acid in CH_2Cl_2 (209 μl, 17.38 mM), HATU in CH_2Cl_2 (209 μl, 17.38 mM), HBTU in CH_2Cl_2 (209 μl, 17.38 mM), and EDC · HCl in CH_2Cl_2 (209 μl, 17.38 mM) were added to each tube containing CH_2Cl_2. DIPEA (1.6 μl, 9.19 μmol) was added to the six tubes, all of which were vortexed for 6 h and then spun at 12,000 rpm for 2 min. The supernatant was removed, and the precipitated material was washed with DMF (2 × 0.5 ml) and MeOH (2 × 0.5 ml). Removal of nucleobase-protecting groups and cleavage from the solid support were achieved by suspending the material in aq. NH_3 (0.5 ml, 28 – 30%) and incubation at 55° for 16 h. The resin was filtered off, and the product (in the filtrate) was purified by reversed-phase (RP) HPLC, detritylated, and precipitated from abs. EtOH as described above. The functionalization efficiencies were determined *via* RP-HPLC by calculating the integrals of the peaks of unfunctionalized and functionalized oligonucleotides, resp. (Fig. S9 – S10; *Supporting Information*).

Functionalization of **ON2** – **ON14**. A similar procedure as described above for **ON1** was employed for **ON2** – **ON10** with the following amounts used: solid-phase-bound **ON2** – **ON10** (12 mg, 0.4 μmol); DMF (240 μl); HATU (628 μl, 17.38 mM); pyrene-1-carboxylic acid (628 μl, 17.38 mM); DIPEA (4.8 μl, 27.5 μmol). The tubes were vortexed for 6 h, and their contents were treated with aq. NH_3 (1 ml, 28 – 30%, 55°, 16 h), and purified by RP-HPLC afford **ON32** – **ON40**. The compositions and purities were verified by MALDI-MS and anal. ion-exchange HPLC, resp., as described above (Table S2 and Fig. S12 – S20; *Supporting Information*).

Thermal Denaturation Measurements. All measurements were performed on a UV/VIS spectrophotometer equipped with a *Peltier*-temp. controller in a medium salt buffer (100 mM NaCl, 0.1 mM EDTA, and adjusted to pH 7.0 with 10 mM NaH_2PO_4/5 mM Na_2HPO_4) at an ON concentration of 1.0 μM pr. strand (calc. from OD_{260} measurements using extinction coefficients from [53]). Prior to each measurement, each mixture was heated to 60° and cooled to the starting temp. of the experiment. The temp. range in each experiment was 5.0 – 60° with a temp. gradient ramp of 1.0°/min. For samples with

low T_m, values the starting temp. was reduced to 3.0° and a gradient of 0.5°/min was used. Thermal denaturation temps. (T_m value/°) were calculated as the maximum of the first derivative of thermal denaturation curves (A_{260} *vs.* temp.). Reported T_m values are averages of at least two measurements within ±1.0°.

Fluorescence Measurements. All measurements were performed on a *PerkinElmer LS 55* luminescence spectrometer equipped with a *Peltier* temp. controller (set to 5°) in a medium salt buffer (100 mM NaCl, 0.1 mM EDTA, and adjusted to pH 7.0 with 10 mM NaH_2PO_4/5 mM Na_2HPO_4) at an ON concentration of 1.0 μM pr. strand (calc. from OD_{260} measurements using extinction coefficients from [53]). Emission was measured from 360 to 600 nm after excitation at 352 nm with an excitation slit of 4.0 nm and an emission slit of 2.5 nm. The reported spectra are an average of five scans and corrected for background emission from the buffer.

Molecular Modeling. Structures (including **ON31**, **ON32**, **ON35**, **ON37**, and **ON38**) were built inside the *MacroModel* software suite V9.2 [58]. ONs were built as standard B-DNA for DNA:DNA duplex and as A-type for DNA:RNA hybrid duplexes. The charges of the phosphodiester backbone were neutralized with sodium ions placed 3 Å from the two non-bridging O-atoms, and restrained to this distance by a force constant of 100 kJ/mol Å^2. For all minimizations, a *Polack–Ribiere* conjugate gradient method (convergence criteria, 0.1 kJ/mol Å^2) was used. All calculations were performed with a GB/SA solvation model [59][60] using the all-atom AMBER* force field as implemented in *MacroModel V9.2* [58]. Cut-off was set to extended (*Van der Waals*, 8.0 Å; electrostatic, 20.0 Å; and H-bond, 4.0 Å) and electrostatic treatment set to be force field defined. A built structure was minimized prior to a Monte Carlo conformational search (MCMM), sampling the conformational space by random variation of bonds marked in red (Fig. S4; *Supporting Information*; sampling 1,000 structures). The 1000 generated structures were minimized and the lowest-energy structure was used as starting structure for a stochastic dynamics (SD) simulation as follows.

Simulation time, 10 ns; simulation temp., 300 K; time step, 2.2 fs; an equilibration time 10 ps and SHAKE algorithm set to bonds to H-atoms. Convergence threshold were set to 0.05 kJ/mol Å^2. During those 10 ps, 500 structures are sampled and minimized to give the global minima structure, which was used for final structural assessment.

REFERENCES

[1] 'Antisense Drug Technology', Ed. S. T. Crooke, Marcel Dekker Inc., New York, 2001.
[2] K. V. Gothelf, T. H. LaBean, *Org. Biomol. Chem.* **2005**, *3*, 4023.
[3] E. M. Boon, J. K. Barton, *Curr. Opin. Struct. Biol.* **2002**, *12*, 320.
[4] C. J. Leumann, *Bioorg. Med. Chem.* **2002**, *10*, 841.
[5] N. C. Seeman, *Trends Biochem. Sci.* **2005**, *30*, 119.
[6] M. Shionoya, *Macromol. Symp.* **2004**, *209*, 41.
[7] A. P. Silverman, E. T. Kool, *Chem. Rev.* **2006**, *106*, 3775.
[8] J. Goodchild, *Bioconjugate Chem.* **1990**, *1*, 165.
[9] N. M. Bell, J. Micklefield, *ChemBioChem* **2009**, *10*, 2691.
[10] J. K. Bashkin, E. I. Frolova, U. S. Sampath, *J. Am. Chem. Soc.* **1994**, *116*, 5981.
[11] D. E. Bergstrom, N. P. Gerry, *J. Am. Chem. Soc.* **1994**, *116*, 12067.
[12] G. B. Dreyer, P. B. Dervan, *Proc. Natl. Acad. Sci. U.S.A.* **1985**, *82*, 968.
[13] J. Hall, D. Hüsken, R. Häner, *Nucleosides, Nucleotides Nucleic Acids* **1997**, *16*, 1357.
[14] D. J. Hurley, Y. Tor, *J. Am. Chem. Soc.* **2002**, *124*, 3749.
[15] T. Ihara, M. Nakayama, M. Murata, K. Nakano, M. Maeda, *Chem. Commun.* **1997**, 1609.
[16] D. Magda, S. Crofts, A. Lin, D. Miles, M. Wright, J. L. Sessler, *J. Am. Chem. Soc.* **1997**, *119*, 2293.
[17] R. C. Mucic, M. K. Herrlein, C. A. Mirkin, R. L. Letsinger, *Chem. Commun.* **1996**, 555.
[18] Y. Tor, *C. R. Chim.* **2003**, *6*, 755.
[19] C. J. Yu, Y. J. Wan, H. Yowanto, J. Li, C. L. Tao, M. D. James, C. L. Tan, G. F. Blackburn, T. J. Meade, *J. Am. Chem. Soc.* **2001**, *123*, 11155.

[20] A. R. Pike, L. C. Ryder, B. R. Horrocks, W. Clegg, B. A. Connolly, A. Houlton, *Chem. – Eur. J.* **2005**, *11*, 344.
[21] C. Gosse, A. Boutorine, I. Aujard, M. Chami, A. Kononov, E. Cogne-Laage, J. F. Allemand, J. Li, L. Jullien, *J. Phys. Chem. B* **2004**, *108*, 6485.
[22] M. Manoharan, L. K. Johnson, K. L. Tivel, R. H. Springer, P. D. Cook, *Bioorg. Med. Chem. Lett.* **1993**, *3*, 2765.
[23] R. G. Shea, J. C. Marsters, N. Bischofberger, *Nucleic Acids Res.* **1990**, *18*, 3777.
[24] E. Bonfils, C. Depierreux, P. Midoux, N. T. Thuong, M. Monsigny, A. C. Roche, *Nucleic Acids Res.* **1992**, *20*, 4621.
[25] S. K. Datta, H. J. Cho, K. Takabayashi, A. A. Horner, E. Raz, *Immunol. Rev.* **2004**, *199*, 217.
[26] J. J. Hangeland, J. T. Levis, Y. C. Lee, P. O. P. Tso, *Bioconjugate Chem.* **1995**, *6*, 695.
[27] M. Iyer, J. C. Norton, D. R. Corey, *J. Biol. Chem.* **1995**, *270*, 14712.
[28] C. H. Tung, S. Stein, *Bioconjugate Chem.* **2000**, *11*, 605.
[29] I. Walker, W. J. Irwin, S. Akhtar, *Pharm. Res.* **1995**, *12*, 1548.
[30] T. S. Zatsepin, D. A. Stetsenko, A. A. Arzumanov, E. A. Romanova, M. J. Gait, T. S. Oretskaya, *Bioconjugate Chem.* **2002**, *13*, 822.
[31] S. Ercelen, A. S. Klymchenko, A. P. Demchenko, *Anal. Chim. Acta* **2002**, *464*, 273.
[32] G. S. Jiao, K. Burgess, *Bioorg. Med. Chem. Lett.* **2003**, *13*, 2785.
[33] H. Maeda, T. Maeda, K. Mizuno, K. Fujimoto, H. Shimizu, M. Inouye, *Chem. – Eur. J.* **2006**, *12*, 824.
[34] A. D. Malakhov, M. V. Skorobogatyi, I. A. Prokhorenko, S. V. Gontarev, D. T. Kozhich, D. A. Stetsenko, I. A. Stepanova, Z. O. Shenkarev, Y. A. Berlin, V. A. Korshun, *Eur. J. Org. Chem.* **2004**, 1298.
[35] A. Misra, S. Mishra, K. Misra, *Bioconjugate Chem.* **2004**, *15*, 638.
[36] V. A. Ryabinin, A. S. Butorin, K. Elen, A. Y. Denisov, D. V. Pyshnyi, A. N. Sinyakov, *Russ. J. Bioorg. Chem.* **2005**, *31*, 146.
[37] S. K. Silverman, T. R. Cech, *Biochemistry* **1999**, *38*, 14224.
[38] A. S. Boutorine, H. Tokuyama, M. Takasugi, H. Isobe, E. Nakamura, C. Helene, *Angew. Chem., Int. Ed.* **1994**, *33*, 2462.
[39] J. G. Harrison, S. Balasubramanian, *Bioorg. Med. Chem. Lett.* **1997**, *7*, 1041.
[40] M. Manoharan; K. L. Tivel; P. D. Cook, *Tetrahedron Lett.* **1995**, *36*, 3651.
[41] M. Manoharan, L. K. Johnson, C. F. Bennett, T. A. Vickers, D. J. Ecker, L. M. Cowsert, S. M. Freier, P. D. Cook, *Bioorg. Med. Chem. Lett.* **1994**, *4*, 1053.
[42] D. H. Bradley, M. M. Hanna, *Tetrahedron Lett.* **1992**, *33*, 6223.
[43] V. A. Korshun, I. A. Prokhorenko, S. V. Gontarev, M. V. Skorobogatyi, K. V. Balakin, E. V. Manasova, A. D. Malakhov, Y. A. Berlin, *Nucleosides Nucleotides* **1997**, *16*, 1461.
[44] A. Okamoto, K. Kanatani, I. Saito, *J. Am. Chem. Soc.* **2004**, *126*, 4820.
[45] M. J. Robins, P. J. Barr, *Tetrahedron Lett.* **1981**, *22*, 421.
[46] K. Sonogashira, Y. Tohda, N. Hagihara, *Tetrahedron Lett.* **1975**, *50*, 4467.
[47] P. Kocalka, N. K. Andersen, F. Jensen, P. Nielsen, *ChemBioChem* **2007**, *8*, 2106.
[48] M. Raunkjær, K. F. Haselmann, J. Wengel, *J. Carbohydr. Chem.* **2005**, *24*, 475.
[49] K. Bondensgaard, M. Petersen, S. K. Singh, V. K. Rajwanshi, R. Kumar, J. Wengel, J. P. Jacobsen, *Chem. – Eur. J.* **2000**, *6*, 2687.
[50] L. B. Jørgensen, P. Nielsen, J. Wengel, J. P. Jacobsen, *J. Biomol. Struct. Dyn.* **2000**, *18*, 45.
[51] J. Gierlich, G. A. Burley, P. M. E. Gramlich, D. M. Hammond, T. Carell, *Org. Lett.* **2006**, *8*, 3639.
[52] H. M. Pfundheller, A. M. Sørensen, C. Lomholt, A. M. Johansen, T. Koch, J. Wengel, in 'Methods in Molecular Biology: Oligonucleotide Synthesis: Methods and Applications', Ed. P. Herdewijn, Humana, Totawa, 2005, Vol. 288, p. 127.
[53] G. M. Blackburn, M. J. Gait, D. Loakes, D. M. Williams, 'Nucleic Acids in Chemistry and Biology', 3nd edn., The Royal Society of Chemistry, Cambridge, 2006, pp. 13 – 75, 143 – 166.
[54] F. M. Winnik, *Chem. Rev.* **1993**, *93*, 587.
[55] E. Valeur, M. Bradley, *Chem. Soc. Rev.* **2009**, *38*, 606.
[56] Y. J. Seo, J. H. Ryu, B. H. Kim, *Org. Lett.* **2005**, *7*, 4931.

[57] T. S. Kumar, A. S. Madsen, M. E. Østergaard, S. P. Sau, J. Wengel, P. J. Hrdlicka, *J. Org. Chem.* **2008**, *74*, 1070.
[58] MacroModel, Version 9.2, S., LLC New York, 2011.
[59] S. J. Weiner, P. A. Kollman, D. A. Case, U. C. Singh, C. Ghio, G. Alagona, S. Profeta Jr., P. Weiner, *J. Am. Chem. Soc.* **1984**, *106*, 765.
[60] S. J. Weiner, P. A. Kollman, D. T. Nguyen, D. A. Case, *J. Comput. Chem.* **1986**, *7*, 230.

Received April 21, 2014